Paper

IJASS
International Journal of
Aeronautical and Space Sciences

Wing Design Optimization for a Long-Endurance UAV using FSI Analysis and the Kriging Method

Seok-Ho Son*

R&D Engineering Team, PIDO TECH Inc., Seoul 04763, Republic of Korea

Byung-Lyul Choi**

Engineering Consulting Team, PIDO TECH Inc., Seoul 04763, Republic of Korea

Won-Jin Jin***

Depart. of Aviation Maintenance Engineering, Far East University, Chungbuk 27601, Republic of Korea

Yung-Gyo Lee** and Cheol-Wan Kim*****

Aerodynamics Team, Korea Aerospace Research Inst., Dajeon 34133, Republic of Korea

Dong-Hoon Choi****

School of Mechanical Engineering, Hanyang University, Seoul 04763, Republic of Korea

Abstract

In this study, wing design optimization for long-endurance unmanned aerial vehicles (UAVs) is investigated. The fluid-structure integration (FSI) analysis is carried out to simulate the aeroelastic characteristics of a high-aspect ratio wing for a long-endurance UAV. High-fidelity computational codes, FLUENT and DIAMOND/IPSAP, are employed for the loose coupling FSI optimization. In addition, this optimization procedure is improved by adopting the design of experiment (DOE) and Kriging model. A design optimization tool, PIAnO, integrates with an in-house codes, CAE simulation and an optimization process for generating the wing geometry/computational mesh, transferring information, and finding the optimum solution. The goal of this optimization is to find the best high-aspect ratio wing shape that generates minimum drag at a cruise condition of $C_L = 1.0$. The result shows that the optimal wing shape produced 5.95 % less drag compared to the initial wing shape.

Key words: Long endurance UAV(unmanned aerial vehicle), CFD(computational fluid dynamics), FSI(fluid-structure integration) analysis, Design optimization, Kriging method

Nomenclature

α : Angle of attack
$\hat{\beta}$: Coefficient of regression
C_L : Coefficient of drag
C_D : Coefficient of lift
$f(\mathbf{x})$: Global model

Γ : Dihedral angle
λ : Taper ratio
$\mathbf{r}$: Correlation vector
R : Correlation function
$\mathbf{R}$: Correlation matrix
V : Velocity (m/s)
$\mathbf{x}$: Design variables

(cc)

    * Ph. D
   ** Ph. D
  *** Professor
 **** Ph. D
***** Ph. D
****** Professor, Corresponding author: dhchoi@hanyang.ac.kr

$y(\mathbf{x})$: Exact response model
$\hat{y}(\mathbf{x})$: Approximated response model
$Z(\mathbf{x})$: Local deviation model

1. Introduction

The importance of long-endurance unmanned aerial vehicles (UAVs) in future airfields will be growing due to their versatility in many applications, such as executing strategic reconnaissance, providing telecommunication links, and helping in metrological research, forest fire detection, and disaster monitoring. Therefore, design optimization techniques for long-endurance UAVs have been investigated to improve their flight performance and to reduce the development effort. Rajagopal et al. [1-2] proposed a multi-disciplinary design optimization (MDO) for optimizing the conceptual design of a long-endurance UAV with the panel method code, XFLR5. Park et al. [3] employed a simple multi-objective genetic algorithm to find an optimum airfoil shape for a long-endurance UAV.

High-aspect ratio wings of a long-endurance UAV are needed to minimize the induced drag and easily cause wing deflection and deformation during flight [4, 5]. This tendency during flight can cause incorrect prediction results if aerodynamic analysis is performed assuming a rigid wing. Therefore, fluid -structure integration (FSI) analysis must be used in wing design optimization in order to simulate a more accurate and realistic interaction between the aerodynamic loads and the structural components of the aircraft wing.

FSI has two approaches: close coupling and loose coupling [6]. The close coupling approach requires large computational resources since it reformulates and resolves the numerical equations by combining the fluid and structural motion simultaneously. The second approach, loose coupling, deals with only external interactions between the aerodynamic and structural models. Therefore, many researchers have applied the loose coupling FSI to optimize an UAV wing design. For instance, Gonzalez et al. applied loose coupling multi-physics to a long-endurance UAV wing design using XFOIL/ MSES/ NSC2ke and NASTRAN for aerodynamic and structural analyses, respectively [7].

The meta-model techniques, such as the Kriging model, support vector regression (SVR) and artificial neural network (ANN), contribute to simplifying the wing design optimization procedure and produce optimum results without a large amount of expensive simulation. Consequently, the meta-model techniques like SVR and ANN have been incorporated into the UAV aircraft design, especially in the design of their wing components.

Lee et al. suggested the design optimization of a long-endurance UAV wing by using loose coupling FSI analysis and the ANN technique [8]. Lam et al. studied an integrated multi-objective optimization algorithm based on the Kriging method to investigate aerodynamically or structurally optimized transonic wings [9].

In this study, we optimized the design procedure using FSI analysis and the Kriging method. The goal of this study is finding the optimized shape of a high-aspect ratio wing planform having minimum drag for an electrically powered long-endurance UAV. Loose coupling FSI analysis is performed with high-fidelity computational aerodynamic and structural analysis codes, FLUENT and DIAMOND/ IPSAP. These analyses simulate realistic aeroelastic behaviors of the long endurance UAV wing. We especially introduce the design guidelines in which design variables influence the system response of UAV. In addition, we suggest that how to find the optimum solution efficiently though the optimization techniques: design of experiment (DOE) and Kriging method. Finally, we propose the optimum solution to improve the efficiency and accuracy of the long endurance UAV.

2. Optimization Procedure

2.1 FSI analysis

The wing shape of a flying airplane experiences deformations due to the wing's aerodynamic load (the wing is the main source of lift force). The aeroelastic deformation of aircraft wings are usually presented by an upward deflection and a twist motion. Therefore, aerodynamic analysis based on rigid wing shapes could lead to incorrect results.

To avoid these, we use an FSI analysis that considers the coupling effects of an aerodynamic load as well as structural deformation. The computation results of an external aerodynamic load are distributed on the wing surface. Structural analysis of the designed component layouts and material properties of external and internal wing structures is carried out to calculate the amount and direction of deformation caused by the aerodynamic effect. Fig. 1 shows the design procedure of the FSI analysis in this study. The aerodynamic and structural analyses are separately performed in computational fluid dynamics (CFD) and computational structural dynamics (CSD) modules, respectively. This procedure in Fig. 1 is the loose coupling FSI.

The aerodynamic analysis module consisted of GAMBIT [10], T-GRID [11], and FLUENT [12]. FLUENT is a commercial CFD code that uses the Euler solver and Navier-

Stokes solver to simulate the aerodynamic loads. To validate the computation results of this CFD code, the aerodynamic performance are simulated for a UAV (EAV-2), which has similar configuration to the aircraft investigated in this study: the same fuselage, airfoil, and empennage. And the results are compared to the flight test data [13] as presented in Fig. 2. The Navier-Stokes solver is applied, and the same speed and same Reynolds numbers are considered. Also, additional drag from the propeller slipstream is simulated by using the fan-disk model. From the figure we can see that the CFD code is properly predicting the lift and drag characteristics of the UAV.

GAMBIT is a modeling and mesh-generation tool for simulated surfaces of UAV wing. T-GRID is volume-mesh software for three-dimensional airflow space over aircraft surfaces. The total number of mesh nodes on the wing upper and lower surfaces is 5040. Although only the wing is the target of our analysis and optimization, the fuselage and empennage are also included in CFD analysis to take into account the interference effects on the wing. In this way, CFD analysis is performed for a full-scale aircraft. An example of

mesh generation for UAV surfaces is shown in Fig. 3.

In this study, the Euler solver of the FLUENT code is used for the computation of aerodynamic loading. Although the accuracy of the calculation may be reduced compared to the Navier-Stokes solver, the computation time can be significantly reduced by using the Euler solver, without having to include the simulation of boundary layer and viscous effects. Furthermore, the Euler method is considered to be acceptable in this study since the pressure force, which is a main source of the wing deformation, can be accurately predicted by assuming an inviscid flow. Other parameters of the analysis are, the designed cruise speed, substantially low at V = 10m/s, and moderate angles of attack (α = 2 and 4°). Both of these prevent a severe flow separation, which amplify any viscous effects. Not having to simulate the boundary layers, thus eliminating them, contributes to minimizing the number of mesh cells. This facilitates computation speed, and thereby reduces computation time. This is important because numerous cases with various optimization design variables must be computed within the effective time. The CSD analysis is performed using open-source software called the Finite-Element Method (FEM), DIAMOND/IPSAP [14]. The model for structural analysis is presented in Fig. 4. It has 2 spars, 5 ribs and skin, and these parts are put together by manufacturing structure.

The material properties of each structural component are assumed carbon-fiber composite materials that are commonly used for UAV structures. The meshes for the CFD analysis are also dedicated to CSD analysis. For structural analysis, the mesh aspect ratio problem is controlled by increasing the wing spanwise mesh number.

Also, two in-house codes, one is in CFD module and the other is in CSD module, are included in this FSI procedure as shown in Fig. 1. The in-house code in the CFD module does two things. First, it calculates geometric parameters to generate the geometry and mesh of initial wing planform. It does this according to any design variables used in the first FSI iteration. Second, it defines the deflection of the wing
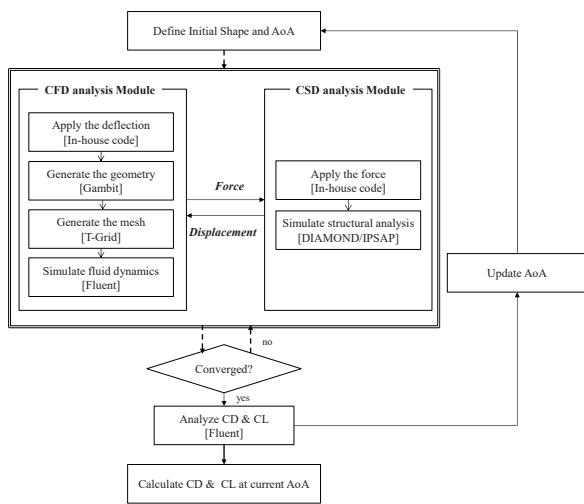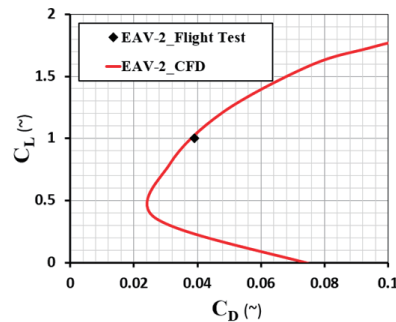

Fig. 1. Fluid-structure interaction (FSI) analysis procedure

(a) EAV-2   (b) Drag polar

Fig. 2. Validation of CFD analysis for EAV-2 aerodynamic performance with flight test data [13] (FLUENT, Re=2.8×10^5)

planform from the CSD analysis to update the geometry and mesh of the wing at each FSI iteration. The in-house code in the CSD module also generates the initial wing shape as defined design variables at the first FSI iteration, and it distributes aerodynamic forces on the wing surface from the CFD analysis onto the structural wing meshes. All of this FSI procedure is monitored and controlled by a process of integration using PIAnO software [15], a design optimization tool.

The procedure of the FSI used in this study begins with initial wing geometry and a wing surface generated by GAMBIT. Then the volume meshes are generated by T-GRID. Next, the CFD analysis is performed using FLUENT; in this, and an aerodynamic load on each node of meshes is transferred to, and distributed on, the corresponding nodes of the structural meshes of DIAMOND/IPSAP for the CSD analysis.

In the second procedure, the amount of wing upward deflection, in terms of wing-tip displacement, is calculated from aerodynamic loads as well as dead loads on the wing. The geometrical data for wing deflections are transferred into GAMBIT again, and the initial wing geometry is updated in

GAMBIT. New meshes are then generated for the deflected wing geometry, and new aerodynamic loads and resulting new displacements are calculated. This iteration process continues until the amount of wing-tip displacement is satisfied with the convergence condition as follows as Eq. 1:

$$f_i - f_{i-1} \leq \varepsilon_f \quad or \quad \delta_i - \delta_{i-1} \leq \varepsilon_\delta \tag{1}$$

where f and δ is a force and displacement, respectively. The subscript i is a current iteration.

This procedure is a two-way FSI analysis and it is mostly completed within 4 to 5 iterations. Fig. 5 shows an example of the FSI convergence history for displacement, and changed aerodynamic characteristics after the two-way FSI analysis. As shown in Fig. 5(b), the initial wing geometry produces a lift of $C_L = 1.2639$ at an angle of attack of 4°, and the deflected wing, after convergence, generates a reduced lift of $C_L = 1.2600$.

2.2 Design of Experiments

The design of experiments (DOE) method is a scientific approach to carry out the experiments most efficiently
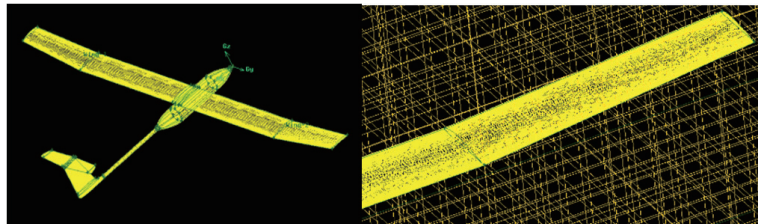

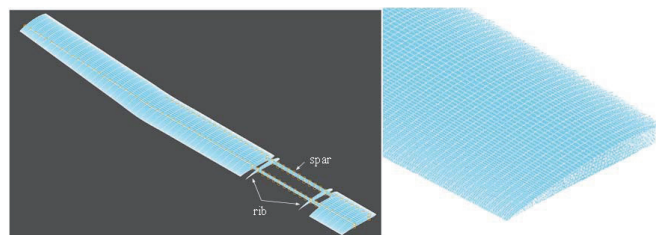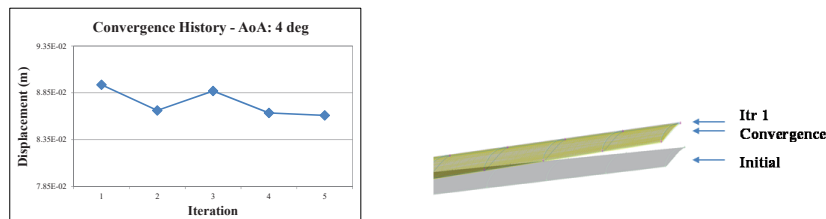Fig. 3. Surface meshes for CFD analysis

Fig. 4. Structural model for CSD analysis

(a) FSI convergence history for displacement   (b) Wing deflection with respect to lift and drag change

Fig. 5. Example of FSI convergence history and wing deflection($\alpha = 4°$, taper ratio $\lambda = 0.7$, dihedral angle $\Gamma = 4°$)

and to simulate the computational system using statistical methods. The DOE is used to determine which design variables have an effect on a response value, and, thus, which design variables should be selected as the best point. Of the many methods for generating sampling points, we choose these: full factorial design (FFD), central composite design (CCD), and optimal latin-hyper cube design (OLHD).

In this study, we employ a 3-level FFD design method for a two design variables, which 2 design variables arranged at 3 different factorial experiment point in Fig. 6 [16]. Due to the filling of sampling points in the design space, 3-level FFD can be represented by the objective function within an entire design space. According to 3-level FFD, a total of 18 simulations (3 taper ratios, 3 dihedral angles, and 2 angles of attack) are carryout by the FSI analysis. Then using the interpolation method at each sampling point, we calculate the objective function, using the values of C_D at the target lift of $C_L = 1.0$

2.3 Kriging Method

Meta-modeling is a method of approximating a real system response efficiently based on the DOE. For wing design optimization, even a single FSI analysis requires a large amount of computation time, and a design optimization with FSI analysis iteratively is very time-consuming. In order to find the optimum wing shape efficiently, the objective function, C_D at $C_L = 1.0$, is approximated by a Kriging method.

The Kriging method is composed of the combination of a global model and a local deviation. An equation of the Kriging model is defined as:

$$y(\mathbf{x}) = f(\mathbf{x}) + Z(\mathbf{x}) \tag{2}$$

where $\mathbf{x}$ is a vector of design variables, $y(\mathbf{x})$ is a black function at the interested point, and $f(\mathbf{x})$ is a global model at $\mathbf{x}$. $Z(\mathbf{x})$ is assumed to be a realization of a stationary Gaussian process with zero mean, sigma square variance, and nonzero covariance. The covariance matrix of $Z(\mathbf{x})$ is defined as Eq. 3:

$$Cov\left[Z(\mathbf{x}_i), Z(\mathbf{x}_j) \right] = \sigma^2 \mathbf{R}\left[R(\mathbf{x}_i, \mathbf{x}_j) \right] \quad i,j = 1,2,\dots nexp, \tag{3}$$
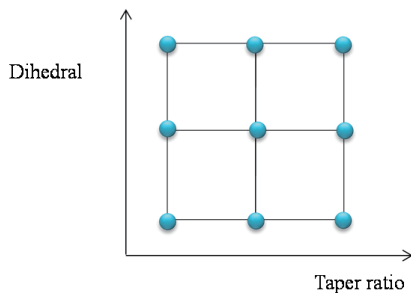
where $\mathbf{R}$ is a correlation matrix and R is a correlation function between any two sampling points in the number of experiment points (nexp).

In general, let $\hat{y}(\mathbf{x}^*)$ be assumed a best linear unbiased predictor (BLUP) of $\hat{y}(\mathbf{x}^*)$ at the point of interest $\mathbf{x}^*$ as follows Eq. 4:

$$\hat{y}(\mathbf{x}^*) = \mathbf{f}^t(\mathbf{x}^*)\hat{\boldsymbol{\beta}} + \mathbf{r}(\mathbf{x}^*)^t \mathbf{R}^{-1}(\mathbf{y} - \mathbf{F}\hat{\boldsymbol{\beta}}), \tag{4}$$

where $\hat{\boldsymbol{\beta}} = (\mathbf{F}^t \mathbf{R}^{-1} \mathbf{F})^{-1} \mathbf{F}^t \mathbf{R}^{-1} \mathbf{y}$, a coefficient of regression, and is estimated by a generalized least square method. The function $\mathbf{r}(\mathbf{x}^*) = \left[R(\mathbf{x}^*, \mathbf{x}_1) \quad \cdots \quad R(\mathbf{x}^*, \mathbf{x}_{nexp}) \right]^t$ is a correlation vector between the interested point $\mathbf{x}^*$ and existing sampling points. For the correlation matrix and correlation vector, the correlation parameters can be estimated by maximizing the concentrated conditional log likelihood function as shown in Eq. 5 [17].

$$\ln L = -\left(nexp \cdot \ln \hat{\sigma}^2 + \ln |\mathbf{R}| \right) \tag{5}$$

2.4 Application of FSI to the wing planform optimization

In this study, optimization of a wing planform is performed to find the optimized values of the two design variables, a taper ratio (λ) and a dihedral angle (Γ). The objective function of this optimization study is the minimum C_D of the aircraft at $C_L = 1.0$. The lift coefficient of the aircraft, $C_L = 1.0$, is the design lift of this study for a long-endurance cruise condition. As shown in Fig. 7, the initial wing planform is consisted of two parts, and the optimization process is applied to the only outboard section (part 2) that starts at the 65% spanwise station. Therefore, the taper and dihedral angle are changed for this outboard section. The initial value of taper ratio and dihedral angels is $\lambda = 0.8$ and $\Gamma = 4°$, respectively. The lower and upper bounds of the taper ratios are 0.7 and 1.0, respectively, and the dihedral angles are +8° and -8°, as presented in Table 1. Wing area and wing root chord are defined and fixed as 2.0 m^2 and 0.32 m, based on a conceptual aircraft design procedure of Advanced Aircraft Analysis (AAA) [18]. Therefore, varying taper ratio with the fixed-wing area results in changes of wing aspect ratio: if

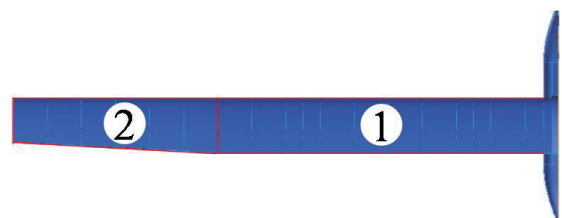Fig. 6. The 3-level full factorial design of two design variables

Fig. 7. Initial wing planform and optimized outboard section

the taper ratio decreases, wing aspect ratio increases. In general, higher aspect ratio (lower taper ratio) wing requires structural reinforcement. Therefore, the taper ratio below $\lambda = 0.7$ is not considered since a lower-taper ratio increases the structural weight of a wing. The $\lambda = 0.8$ is corresponding to AR=20, which is already a high aspect ratio in the practical wing structural design. The design limits for the dihedral angles ($8° \leq \Gamma \leq 8°$) are defined due to the similar reason. Also note that even though the dihedral angle controls the lateral stability of aircraft, it is only considered as a design variable to optimize such that it could affect the wing's aerodynamic performance coupled with the effect of wing deflection.

Two angles of attack, $\alpha = 2$ and $4°$, are considered, and this angle range covers the expected cruise angle of attack. As mentioned above, the optimization problem of this study is that the objective function (a minimum drag, C_D) with constant lift ($C_L = 1.0$) is obtained by the taper ratio (λ) and the dihedral angle (Γ). We try to optimize the taper ratio and dihedral angle so that they minimize C_D at $C_L = 1.0$ as follows in Eq. 6.

$$\begin{aligned} Find \quad & \lambda, \Gamma \\ Minimize \quad & C_D @ (C_L = 1.0) \end{aligned} \qquad (6)$$

The optimization process based on FSI analysis requires a large amount of time and computational resource because the FSI analysis must be simulated at every iteration of a new

case. To improve the procedure efficiency, we optimize by carrying out DOE and the Kriging method. An approximate optimization problem is defined as follows Eq. 7:

$$\begin{aligned} Find \quad & \lambda, \Gamma \\ Minimize \quad & \hat{C}_D @ (\hat{C}_L = 1.0) \end{aligned} \qquad (7)$$

where $\hat{C}_D$, $\hat{C}_L$ is an approximated coefficients of drag and lift, both calculated by the Kriging model.

The optimization algorithms we use with DOE, Kriging method and global optimizer, are also automatically executed by using the PIAnO software.

3. Results and discussion

3.1 FSI analysis results

The FSI analysis results for 18 DOE cases are tabulated in Table 2. These cases are differentiated from each other by three different taper ratios, three different dihedral angles, and two angles of attack. The FSI iteration is performed for each case resulting in values of C_L and C_D are presented in Table 2. The value of the objective function, C_D at $C_L = 1.0$, is calculated through an extrapolation using the values of C_L and C_D at $\alpha = 2$ and $4°$, based on the assumption of linear increase of drag within the considered angles of attack. The

Table 1. Design variables with lower, initial, and upper bounds

	Taper Ratio (λ)	Dihedral (Γ)
Lower Bound	0.7	-8°
Initial	0.8	4°
Upper Bound	1.0	8°

Table 2. FSI analysis results for the 18 cases

Case No.	λ (~)	Γ (deg.)	α=2 deg.		α=4 deg.		C_D @ C_L=1.0
			C_L	C_D	C_L	C_D	
1	0.8	4	1.0685	0.0303	1.2612	0.0425	0.0259
2	1.0	4	1.0479	0.0315	1.2390	0.0442	0.0283
3	0.8	8	1.0641	0.0302	1.2580	0.0426	0.0260
4	0.7	4	1.0869	0.0298	1.2808	0.0421	0.0244
5	0.8	-8	1.0603	0.0300	1.2525	0.0422	0.0262
6	1.0	8	1.0448	0.0313	1.2368	0.0439	0.0283
7	0.7	-8	1.0755	0.0294	1.2716	0.0416	0.0248
8	1.0	-8	1.0405	0.0311	1.2314	0.0437	0.0284
9	0.7	8	1.0836	0.0297	1.2741	0.0418	0.0244

values of the objective function serve as main data for design optimization through the Kriging method.

3.2 Effects of design variables and best points

To investigate the effects of two design variables, taper ratio and dihedral angle, on the objective function, we research the analysis of means (ANOM) and the analysis of variance (ANOVA) using the nine sampling points as shown in Table 2. With the ANOM and ANOVA, the effect of all design variables can be systematically investigated and then the weakly influencing design variables can be omitted to carry out the optimization problem efficiently. As the taper ratio increases from -1 level of DOE (taper ratio = 0.7) to +l level (taper ratio = 1), the objective function value also increases as shown in Fig. 8. However, the change of the objective function value is insignificant with respect to changes in the dihedral angle. In addition, the influence of taper ratio on the objective function is over 90 % in Fig. 9. The results of the ANOM in Fig. 8, and ANOVA in Fig. 9 indicate that the taper ratio has a stronger influence on C_D at $C_L = 1.0$ than the dihedral angle.

Using the DOE table, we also can find the best point that the one of DOE points has a minimum (or maximum) objective function while satisfying constraints. In Table 2, we define the 4th sampling point ($\lambda = 0.7$, $\Gamma = 4°$) with the minimum function value ($C_D = 0.2444$) as the best point.
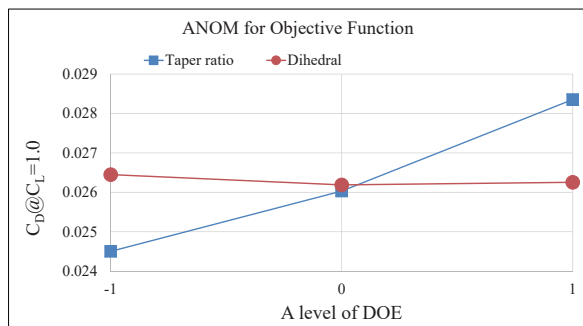

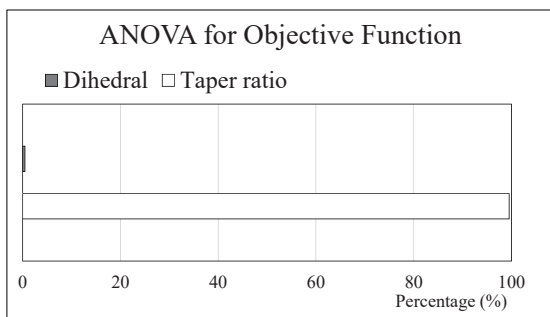Fig. 8. ANOM results for the objective function

Fig. 9. ANOVA results for the objective function

3.3 Design optimization results

The optimization results for the design variables and the objective function from the results of the FSI analysis (Table 2) and the Kriging method are summarized in Table 3. As shown in Table 3, the optimal values of taper ratio and dihedral angle are 0.7 and 5.49, respectively. The approximated value of the objective function from the Kriging method is $C_D = 0.02436$, producing a 5.95 % decrease in drag compared to the drag of the initial shape at $C_D = 0.02590$ within 4 iterations of optimization problem as shown in Fig. 10.

A comparison figure between the initial wing and the optimal wing is shown in Fig. 11. As shown in Fig. 11(a), the taper ratio is decreased from 0.8 (initial) to 0.7 (optimal). When the taper ratio decreases, the length of the wing becomes longer in the direction of chord length to maintain the total area of the wing surface. The optimal dihedral angle is increased up to 5.49°, compared to the initial angle is 4° as shown in Fig. 11(b). To validate the optimization results with the Kriging method, one case of additional FSI analysis is performed based on the optimized design variables, $\lambda = 0.7$ and $\Gamma = 5.49°$. The results in Table 3 suggest the Kriging method properly predicts the objective function since the FSI validation produces a similar value, $C_D = 0.02433$. In addition in Fig. 12, the differences for the C_D values of initial and optimum shapes between the Kriging method and its FSI validation are about 0.1 %. Consequently, the optimized shape of the wing can be efficiently found with both the DOE method and the Kriging method.

4. Conclusions

In this study, we carry out the wing shape optimization of a long-endurance UAV to improve its aerodynamic performance while considering the effect of fluid-structure
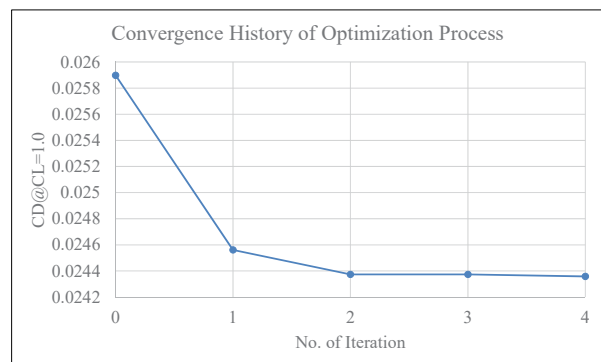

Fig. 10. The convergence history of optimization process

Table 3. Results of optimization problem

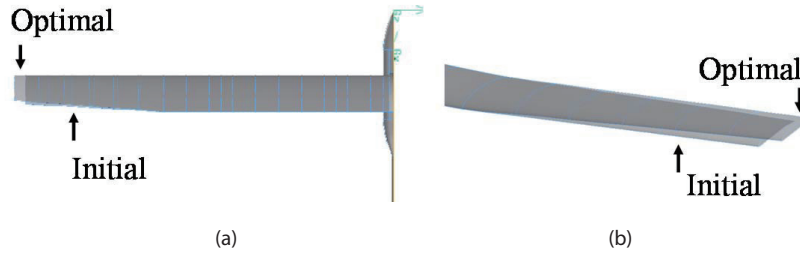|		Lower	Initial	Optimal	Upper
Design Variable	Taper ratio(~)	0.7	0.8	0.7	1
	Dihedral angle(°)	-8	4	5.49	8
Objective (C_D@C_L =1.0)	From the Kriging method		0.02590	0.02436	
	From the FSI validation		0.02590	0.02433	

(a)   (b)

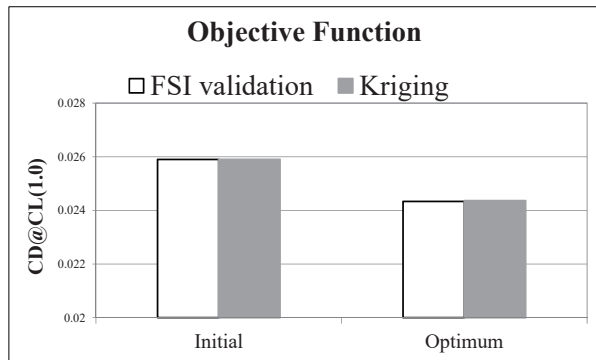Fig. 11. The comparison of the initial and optimal wing shapes

Fig. 12. The comparison of accuracy between the FSI analysis and the Kriging method

interaction. In order to the UAV's aerodynamic performance, its the wing shape, with the design variables, taper ratio and dihedral angle, is optimized to minimize drag, which is the objective function of this study, at the constant lift of $C_L = 1.0$. In addition, the optimization process is facilitated through the DOE and Kriging method.

Among the wing design variables, the taper ratio influences on the objective function more than the dihedral angle. The optimized wing shape of the UAV is represented by the decreased taper ratio ($\lambda = 0.7$) and the increased dihedral angle ($\Gamma = 5.49°$) compared to these variables of the initial wing design. The corresponding decrease in the UAV wing drag is approximately 5.95% ($C_D = 0.02436$), compared to that of the initial wing ($C_D = 0.02590$).

From the fact that the FSI validation shows only 0.1 % difference in the UAV wing drag ($C_D = 0.02433$), we can guarantee that the Kriging method is a good predictor of the FSI analysis.

References

[1] Rajagopal, S. and Ganguli, R., "Conceptual Design of UAV Using Kriging Based Multi-objective Genetic Algorithm", *Aeronautical Journal*, Vol. 112, No. 1137, 2008, pp. 653-662.

[2] Rajagopal, S. and Ganguli, R., "Multidisciplinary Design Optimization of a UAV Wing Using Kriging Based Multi-objective Genetic Algorithm", *50th AIAA/ASME/ASCE/AHS/ASC Structures, Structural Dynamics, and Materials conference*, Palm Springs, California, 2009.

[3] Park, K., Han, J., Lim, H., Kim, B. and Lee, J., "Optimal Design of Airfoil with High Aspect Ratio in Unmanned Aerial Vehicles, *International Journal of Aerospace and Mechanical Engineering*, Vol. 2, No. 4, 2008, pp 177-183.

[4] Jin, W. and Lee, Y., "Drag Reduction Design for a Long-endurance Electric Powered UAV", *International Journal of Aeronautical and Space Sciences*, Vol. 16, No. 2, 2015, pp. 311-324.

[5] Jin, W. J. and Lee, Y., "Computational Analysis of the Aerodynamic Performance of a Long-Endurance UAV", *International Journal of Aeronautical and Space Sciences*, Vol. 15, No. 4, 2014, pp. 374-382.

[6] Kamakoti, R. and Shyy, W., "Fluid-structure Interaction for Aeroelastic Applications", *Progress in Aerospace Sciences*,

Vol. 40, 2004, pp. 535-558.

[7] Gonzalez, L.F., Walker, R., Srinivas, K. and Periaux, J., "Multidisciplinary Design Optimization of Unmanned Aerial Systems (UAS) Using Meta Model Assisted Evolutionary Algorithms", *16th Australasian Fluid Mechanics Conference*, Gold Coast, Australia, 2007.

[8] Lee, S., Park, K., Kim, J., Jeon, S., Kim, K. and Lee, D., "Fluid-Structure Interaction and Design Optimization of HAR Wing for Continuous 24-hour Flight of S-HALE Aircraft", *the proceeding of KSAS*, Vol. 4, 2012, pp. 121-126.

[9] Lam, X., Kim, A., Hoang, A. and Park, C., "Coupled Aerostructural Design Optimization Using the Kriging Model and Integrated Multiobjective Optimization Algorithm", *Journal of Optimization Theory and Applications*, Vol. 142, 2009, pp. 533-556.

[10] GAMBIT Software Package, Ver. 2.4.6, *Ansys Fluent Inc.*, Canonsburg, PA, USA

[11] TGRID Ver. 3.5, *Ansys Fluent Inc.*, Canonsburg, PA, USA

[12] FLUENT Software Package, Ver. 6.3.26, *Ansys Fluent Inc.*, Canonsburg, PA, USA

[13] W. Jin. and Y. G. Lee, "Drag Reduction Design for a Long-endurance Electric Powered UAV", *International Journal of Aeronautical and Space Sciences*, Vol. 16, No. 2, 2015, pp. 311-324.

[14] Diamond user manual, http://www.ipsap.snu.ac.kr, 2008.

[15] PIAnO (Process Integration, Automation and Optimization) User's Manual, Version 2.4, *PIDOTECH Inc.*, 2008.

[16] Son, S., Lee, S. and Choi, D., "Experiment-Based Design Optimization of a Washing Machine Liquid Balancer for Vibration Reduction", *International Journal of Precision Engineering and Manufacturing*, Vol. 13, No. 8, 2012, pp. 1433-1438.

[17] Forrester, A., Sobseter, A. and Keane, A., *Engineering Design via Surrogate Modeling*, John Wiley & Sons, 2008.

[18] Advanced Aircraft Analysis software package, Ver. 3.2, *DARCorporation, Lawrence*, KS, USA